Lawrence Berkeley National Laboratory

Title
Graphitic Carbon Materials for Advanced Sodium-Ion Batteries

Permalink
https://escholarship.org/uc/item/85m9h0mn

Journal
Small Methods, 3(4)

ISSN
2366-9608

Authors
Xu, Zheng-Long
Park, Jooha
Yoon, Gabin
et al.

Publication Date
2019-04-01

DOI
10.1002/smtd.201800227

Peer reviewed

WILEY-VCH

Review

Graphitic carbon materials for advanced sodium ion batteries

Zheng-Long Xu,[1][†] Jooha Park,[1][†] Gabin Yoon,[1] Haegyeom Kim[2] and Kisuk Kang[1]*

Dr. Z. L. Xu, J. Park, G. Yoon and Prof. K. Kang
Department of Materials Science and Engineering, Research Institute of Advanced Materials (RIAM), Seoul National University, 1 Gwanak-ro, Gwanak-gu, Seoul 151-742, Republic of Korea.
E-mail: matlgen1@snu.ac.kr
Dr. H. Kim
Lawrence Berkeley National Laboratory, 1 Cyclotron Rd. Berkeley, CA 94720, USA.

Lithium-ion batteries (LIBs) have dominated the energy storage market for more than two decades; however, the quest for lower-cost battery alternatives is rapidly expanding, especially for large-scale applications. Sodium-ion batteries (SIBs) have recently experienced an impressive resurgence owing to the Earth abundance of sodium resources and the similar electrochemistry of SIBs and the well-established LIBs. Nonetheless, whereas cost-effective and reliable graphite anodes have served as a cornerstone in current LIB technology, one of the major limitations of SIBs has been the inability to exploit graphite as an electrode because of its negligible sodium storage capability. Recently, however, clear progress has been made in preparing high-performance graphitic carbon anodes for SIBs with new findings on the mechanisms of sodium storage. Herein, we aim to review the progress made in understanding the sodium storage mechanisms in graphitic carbon materials and comprehensively summarize the start-of-the-art achievements by surveying the correlations among the type of graphitic material, microstructure, sodium storage mechanisms, and electrochemical performance in SIBs. In addition, perspectives related to practical applications, including the electrolyte, coulombic efficiency, and applicability in sodium-ion full cells, are also presented.

1. Introduction

The ever-growing energy concerns associated with environmental pollution have motivated substantial efforts to explore green and sustainable energy resources such as wind and solar power. However, the intermittent nature of these energy resources place a vital demand on the development of grid-scale energy storage systems (ESSs).[1,2] Rechargeable batteries based on electrochemical energy storage are one of the most promising candidates for this purpose because of their high energy conversion efficiency, design flexibility, manufacturing capability, and wide availability. Since the early 1990s, lithium-ion batteries (LIBs) have become the common choice to power portable electronic devices because of their high energy densities and reliable performance.[3,4] Encouraged by proven success in the portable electric market, LIBs have also been considered promising contenders for penetrating the large-scale ESS field with representative applications such as electric vehicles (EVs) and smart grids. Nevertheless, the surging global market of EVs and the energy demand for grid-scale (MWh or above) ESSs have inevitably raised concerns about the availability and cost of LIBs and lithium resources.[5–7] According to the US Geological Survey (USGS), in 2012, the global consumption of lithium was equivalent to approximately 0.15 million tons of lithium carbonate, whereas in 2018, the worldwide identified reserves were estimated to be 16 million tons.[8] In addition, more than 60% of lithium reserves are geographically concentrated in a few regions,[9] limiting the reliable supply of lithium. Although the availability of lithium resources to meet the future demand of LIBs remains debatable,[8,10,11] the recent leap in the price of lithium carbonate, the main precursor for lithium, suggests that this concern should not be overlooked.[8,10]

Recently, sodium-ion battery (SIB) technology has been extensively investigated as a promising alternative to current LIBs. The concept of SIBs is not new and was primarily investigated in parallel with LIBs in the 1970s and 1980s.[12,13] The working principles of SIBs and LIBs are fundamentally identical that the alkali ion (Li or Na) is transported

2

between two electrode materials to reversibly store and release the electrochemical energy. The differences mainly lie on the larger/heavier Na^+ ion (ionic radius of 1.02 Å and molar mass of 23 g mol^{-1} compared with 0.76 Å and 6.9 g mol^{-1} for a Li^+ ion, respectively) and the higher standard electrode potential for Na^+/Na (−2.71 V *vs*. SHE compared with −3.02 V *vs*. SHE for Li^+/Li), which typically leads to lower energy densities for SIBs than for LIBs.[14] Nevertheless, SIBs potentially possess the merits of energy density per capital over LIBs, especially when considering the readily available sodium resources. Moreover, the rich cathode chemistry involving low-cost transition metals such as Fe and Mn, which leads to better cyclic stability and electrochemical activities compared with those of LIBs,[15,16] encourages the possible development of more cost-effective and reliable cathodes for SIBs. In addition, sodium does not react with aluminum, enabling the use of lighter and less expensive aluminum foil to replace the costly copper-based current collectors for anodes in LIBs. It is expected that borrowing the well-established strategies and techniques for LIBs can accelerate the commercialization of SIBs by taking advantage of the similar electrochemistry of SIBs and LIBs.

The key to the success of SIBs is the development of high-performance electrode materials that can compete with those of LIBs. A wide variety of materials have been investigated for use as SIB cathodes,[15–18] which can be mainly divided into four classes: (i) transition metal oxides (Na_xMO_2, M = transition metal),[19–21] (ii) polyanion-based materials such as phosphates and pyrophosphates (*e.g*., $NaFePO_4$, $Na_3V_2(PO_4)_3$, and $Na_3V_2(PO_4)F_3$),[22–26] (iii) organic materials (*e.g*., $Na_2C_6O_6$),[27–29] and (iv) Prussian blue analogues (*e.g*., $Na_xFe[Fe(CN)_6]$ and $Na_2MnFe(CN)_6$).[30–32] SIB cathodes have exhibited promising electrochemical performance, reaching an energy density of ~600 Wh kg^{-1} and outstanding cyclic capacity retention of ~84% after 500 cycles,[24] suggesting their potential competence to LIB cathodes. In contrast to the ample choices for cathodes, the options for suitable anodes have been rather limited. During the early stage of development, carbon materials such as graphite, petroleum

3

coke, and Shawinigan black were studied for Na storage but exhibited disappointingly low specific capacities of 31 mAh g^{-1} (NaC$_{70}$), 70 mAh g^{-1} (NaC$_{30}$), and 132 mAh g^{-1} (NaC$_{15}$), respectively.[33,34] Dahn and co-workers later observed that hard carbon made from glucose or cellulose could offer a high capacity of approximately 300 mAh g^{-1},[35,36] although the cycle stability was far from sufficient to compete with commercial LIBs. Other potential anode materials have been recently studied including metal alloys (*e.g.*, Sn, Sb, P and Bi)[37–41] and metal oxides/chalcogenides (*e.g.*, Fe$_2$O$_3$, TiO$_2$, SnS$_2$).[14,42,43] These anodes undergo alloying or conversion reactions are capable of delivering higher Na storage capacities; however, the large volume variation associated with Na insertion/extraction typically leads to structural degradation and poor cyclic stability. For example, although phosphorus exhibits an impressively high theoretical capacity of 2595 mAh g^{-1}, only a capacity of 600 mAh g^{-1} with retention of approximately 33% after 140 cycles was reported by Yang *et al*.[41] Nanostructural engineering has often been adopted to improve the cyclic stability and rate capability but is associated with new challenges of low yielding, high cost, and complicated synthesis procedures, which are not acceptable for practical applications.

Various carbonaceous materials have been continuously explored as anodes for SIBs because of their Earth abundance and chemical diversity.[44–49] Extensive research efforts have mostly focused on non-graphitic carbon electrode materials.[46–48] This emphasis was partly due to the thermodynamic instability of Na-graphite intercalation compounds (Na-GICs), as evidenced from recent theoretical studies, which prevent Na intercalation into graphite.[50,51] Although respectable performance with respect to the capacity and cycling stability can be achieved using non-graphitic carbon materials, the low coulombic efficiencies, especially for the first cycle, resulting from the typically large surface area and the risks of Na dendrite formation are regarded as the main drawbacks of these materials.[46–48] Very recently, Kang's group[52] and Adelhelm's group[53] reported that sodium ions can be intercalated and reversibly de-intercalated within the graphite host via a co-intercalation mechanism. This discovery led to

the development of a graphite anode with high reversible Na storage capacities and superior cyclic life. Numerous efforts have since been devoted to studying the reaction mechanisms and conditions for the co-intercalation and improving the electrochemical performance through modification of the materials.[51,54–57] This review is dedicated to undertaking the survey and analysis of state-of-the-art graphitic carbon anodes with respect to their structure, sodium storage mechanisms, and electrochemical performance. Issues related to practical applications, including the electrolyte, coulombic efficiency, and Na-ion full cells, are also discussed. Finally, we examine the major challenges facing SIB anodes for large-scale ESSs and conclude with perspectives.

2. Graphite anodes

2.1 Thermodynamic consideration of sodium-ion intercalation in graphite

Graphite is capable of storing a large amount of Li ions (theoretical capacity of 372 mAh g^{-1}) via intercalation reactions at a redox potential of ~0.1 V *vs*. Li$^+$/Li.[58,59] Graphite can also reversibly form KC$_8$ intercalation compounds, which could potentially be used for rechargeable potassium-ion batteries (KIBs).[60] Moreover, other alkali-metal ions, such as Rb$^+$ and Cs$^+$, have also been reported to be capable of being intercalated into the graphite host.[61,62] It can therefore be expected that sodium ions would also be stored in graphite. However, sodium binary graphite intercalation compounds (*b*-GICs) have hardly been obtained, indicating the negligible solubility of Na in graphite.[33,34,63] Stevens *et al*. reported that sodium insertion into the sites where Li ions occupy graphite was not possible and tends to result in metal deposition on the surface of graphite (**Figure 1**a).[36] After excluding the external contributions from reversible sodium metal stripping and plating, the amount of sodium reversibly intercalated into graphite was very small (~NaC$_{186}$). When heating graphite and sodium metal together at 400 °C,[64] a NaC$_{64}$ compound was obtained, further indicating the low sodium storage capacity in graphite.

To elucidate the origin of the low sodium intercalation capacity in graphite, various theoretical studies have been conducted.[50,51,65–69] An early study by Di Vincenzo *et al*. in 1985[65] claimed that the Na–C interaction was anomalously weak because of the repulsive nature of the Na pseudopotential near the origin, leading to thermodynamically unstable Na-GICs. Nobuhara *et al*.[66] calculated the formation energies for alkali-metal graphite intercalation compounds (AM-GICs) and attributed the energetically unstable Na-GICs to the strong stress of the C–C bond lengths. Liu *et al*.[50] and Wang *et al*.[67] attempted to elucidate the instability of sodium in graphite by deconvoluting the formation energy (E_f) of Na-GICs into the following components using Hess's law:[50] (i) the AM reconstruction energy during the formation of AM-GICs, (ii) the graphite host reconstruction energy during the formation of AM-GICs and (iii) other remaining energies. Although they observed that component (iii) was the dominant reason for the positive value of E_f for Na-GICs, this component is a simple summation of all the energy contributions other than those stemming from the reconstruction of AM and graphite. To obtain a better understanding of the Na instability in Na-GICs, Yoon *et al*. categorized the possible factors having major effects on the formation of AM-GICs,[51] including (i) the energy penalty of metal decohesion, (ii) the contribution of graphite interlayer deviation, and (iii) the local interaction between the AM and a single layer of graphene (Figure 1b). This approach exclusively extracted the local interactions between the AM and graphene layers as the dominant factor, facilitating more precise quantification of the energy contributions. It was demonstrated that factors (i) and (ii) did not display any Na anomaly, as factor (i) was simply determined from the mismatch between atomic sizes of the AM (2.97, 3.63, 4.57, 4.90, and 5.32 Å for Li, Na, K, Rb, and Cs, respectively) and the lattice size of the GICs (4.32 Å for MC_6 and 4.93 Å for MC_8 structures) and factor (ii) was related to the electrostatic repulsion force, which is a function of the interlayer distances of GICs (Figure 1c–d). Therefore, these factors could not explain the peculiar unstable formation of Na-GICs. However, the local binding of a Na ion to a single layer of graphene was uniquely

6

unstable by ~0.5 eV (E_i) compared with those for other AMs (Figure 1e). The trend of E_i was also consistent with that of E_f reported for AM-GICs,[50,51,67] strongly suggesting that the repulsive local interactions between graphene layers and sodium ions dominantly destabilized the Na-GICs, consequently leading to extremely low sodium storage capacities in graphite anodes. It also implies that if the direct local interactions between graphene and sodium ions could be mitigated, graphite would be capable of accommodating sodium ions.

2.2 Intercalation of solvated sodium ion in graphite

Kim *et al*.[52] and Jache *et al*.[53] independently reported the intercalation of sodium in graphite, which could be realized by the co-intercalation mechanism. Jache *et al*.[53] demonstrated that the sodium storage capacity of graphite could increase from near zero in a $NaPF_6$ ethylene carbonate/diethyl carbonate (EC/DEC) electrolyte (**Figure 2**a) to ~100 mAh g^{-1} in a sodium triflate (NaOTf) diglyme electrolyte (Figure 2b); in addition, a high coulombic efficiency of >99.87% was obtained over 1000 cycles (Figure 2c). *Ex situ* X-ray diffraction (XRD) characterization of discharged and charged electrodes revealed a volume expansion of 15% for the co-intercalated graphite. In contrast, Kim *et al*. [52] reported a volume change of ~347% for the co-intercalation of the pristine graphite with the cycle stability for 2500 times. According to Kim *et al*., the interlayer distance of the graphene layers significantly increased from 0.33 nm for pristine graphite to 0.415–0.530 nm after full sodiation from high-resolution transmission electron microscopy (HRTEM). Direct evidence of the co-intercalation was provided by Fourier-transform infrared (FTIR) spectroscopy analysis, which revealed the presence of solvated Na ion in the discharged graphite. The effects of the salt and solvent of the electrolytes were also investigated, demonstrating the negligible dependency on the salts, *e.g.*, $NaPF_6$, $NaClO_4$, and $NaCF_3SO_3$ (Figure 2d) and suggesting the independence of the co-intercalation reactions on the anions in the electrolytes. However, when graphite electrodes were cycled in different electrolyte using different linear ethers, *e.g.*, dimethoxyethane (DME), DEGDME, and tetraethylene glycol dimethyl ether (TEGDME), a noticeable increase of the

7

average Na storage potential from 0.60 to 0.78 V was observed with increasing chain length (Figure 2e). This behavior suggested that the electrolyte solvents participated in the electrochemical reactions, influencing the co-intercalation potentials. The electrochemical analysis revealed that the contributions from the intercalation and capacitive reactions varied at different Na storage stages (Figure 2f).

Following these pioneering works, various graphitic carbon materials, including graphene foam,[56] natural graphite,[70] N330 carbon black,[71] expanded graphite,[72] carbon sheets[73] and graphitic mesocarbon microbead,[74] have been cycled in ether-based electrolytes to examine co-intercalation reactions. Almost all of the materials delivered high reversible capacities, long cycle life, and remarkable high rate capabilities (**Table 1**). One noteworthy example is the use of few-layered graphene foam (FLG) for Na-ion storage via co-intercalation.[56] The FLG material prepared by chemical vapor deposition (CVD) possessed high electrical conductivity, large pores, a high surface area, and a freestanding structure, which were beneficial in securing a large electrolyte/electrode interface for high rate performance. The FLG electrode maintained ~125 mAh g^{-1} (~80% of the maximum capacity) at a rate of 10 A g^{-1} and ~100 mAh g^{-1} (~65% of the maximum capacity) at a rate of 30 A g^{-1} (Figure 2g). Such a high rate capability is among the best for SIBs and was attributed to the fast ion diffusion coefficient (2×10^{-8} to 2×10^{-7} cm^2 s^{-1} during the reactions), the integrity of the materials, and the mitigation of desolvation through solvent co-intercalation. In addition, the FLG electrodes exhibited a high capacity retention of 96% over a long span of 8000 cycles (Figure 2h). There is no doubt that the co-intercalation reactions open a new avenue toward exploiting graphitic carbon materials as anodes for high-power SIBs.

2.3 Conditions and mechanisms for Na co-intercalation in graphite

As mentioned in Section 2.1, the instability of Na-GIC is caused by the unfavorable local environment arising from the Na–graphene local interaction. One plausible approach to negate the unstable interaction is to screen the bare Na ions with molecules such as solvents.

8

Indeed, theoretical calculations have confirmed that the interaction between the Na–solvent complex and graphene layers did not show any peculiar instability because of the inhibited direct Na–graphene interaction. Consequently, the formation energy of Na–DEGDME co-intercalated graphite was calculated to be −0.87 eV,[51] which is much lower than that of *b*-GIC (*e.g*., 0.03 eV for NaC$_6$).[50] This finding suggested that Na intercalation into graphite could be realized using co-intercalation. Yoon *et al*. conducted a series of theoretical calculations to study the solvent dependency of the Na–solvent co-intercalation behavior.[51] They suggested that two conditions were necessary for reversible Na storage in graphite, namely, (i) a large solvation energy of the [Na–solvent]$^+$ complexes to ensure the co-intercalation of the solvent and Na$^+$, and (ii) high lowest unoccupied molecular orbital (LUMO) levels of the [Na–solvent]$^+$ molecules to prevent the decomposition of the intercalated [Na–solvent]$^+$ (**Figure 3**). Typically, compared with carbonate and cyclic ether solvents, linear ether solvents, such as DME, DEGDME, and TEGDME, exhibit a strong solvating behavior because the multiple oxygen atoms in their structure help to stabilize the Na ions. A large solvation energy leads to the stability of [Na–solvent]$^+$ complexes, which aids their co-intercalation into graphite. For the second condition, if the LUMO level of the [Na–solvent]$^+$ complexes (*e.g*., [Na–PC]$^+$) is lower than the Fermi level of graphite, the intercalated [Na–solvent]$^+$ readily accepts an electron from the graphite host, leading to decomposition accompanied by the evolution of gases. This decomposition typically leads to the exfoliation of graphite and the irreversibility of the co-intercalation, as observed in Li–PC systems.[75,76] The calculations performed by Yoon *et al.* revealed that the LUMO levels of [Na–linear ether]$^+$ complexes are mostly higher than the Fermi level of graphite, suggesting the chemical stability of [Na–linear ether]$^+$ in graphite and ensuring the reversible co-intercalation.

The co-intercalation reaction mechanisms have also been intensively investigated using *in-situ* techniques, including *in-situ* synchrotron XRD,[54] Raman,[56] electrochemical dilatometry

9

(ECD),[77] and electrochemical scanning tunneling microscopy (EC-STM) to examine the phase/structure transitions, volume change, and diffusion rate of [Na–solvent]$^+$ in the graphite lattice.[57] Kim *et al.*[54] elucidated the phase evolutions of graphite during co-intercalation using *in-situ* synchrotron XRD. According to the XRD patterns (**Figure 4**a), pristine graphite transformed into multiple new phases and was recovered completely after 1 cycle. The evolution of the XRD patterns clearly indicated the typical staging behaviors. During the initial sodiation steps, graphite underwent one-phase-like reactions with many different staging structures, which sensitively changed with small variation of the Na content. The following phase transformations continued by forming stage 3, stage 2, and stage 1 with further [Na–solvent]$^+$ complex intercalations. During the desodiation steps, reverse phase transformations were observed with a high reversibility. The staging process was also supported by the intensity ratio changes between uncharged and charged graphite (I_{UC}/I_C) detected using the *in-situ* Raman technique.[56] Regarding the co-intercalated graphite structure, the c-lattice distance changed by ~3.4 Å at each stage, and the c-axis distance of stage 1 expanded to 11.62 Å upon the full sodiation (~347% volume change from pristine graphite). The large volume expansion was also observed in chemical co-intercalation of highly oriented pyrolytic graphite (HOPG) using Na metal in ether-based electrolytes, which is in contrast to the 15% volume expansion reported by Jache *et al.*[53,54,57] It was also noted that despite the large volume change, no noticeable structure degradation was detected after cycling. The volume expansion behavior of graphite electrode was further studied by Gokta *et al.*[77] using an *in-situ* ECD technique. The initial sodiation led to a significant increase in the electrode thickness with a volume expansion of ~200%. In the following cycles, the electrode periodically "breathed" with volume changes of 70%–100% (Figure 4b). The decreased volume variation after the first cycle was attributed to the rearrangement of graphite particles. During a single discharge/charge cycle, the electrode expansion was observed to be dependent on the reaction stage rather than the amount of intercalated Na. The volume change for the

discharge plateau at ~0.6 V was more than 50%; however, only 25%–30% (near 40 mAh g^{-1}) of the total charge was gained (Figure 4c). Approximately one third of the electrode charge was obtained below 0.5 V; however, almost no electrode expansion occurred in this region. These observations suggested that the staging behaviors of co-intercalation reactions could be indirectly monitored by measuring the macroscopic dimensional changes of the electrode. Dilatometer studies have also provided evidence that graphite electrodes are highly reversible despite the large changes in the graphite layer spacing. The remarkable stability under significant volume change was attributed to the increased interlayer binding resulting from the positively charged intercalants and chemical stability of [Na–solvent]$^+$ complexes.[78]

Seidl *et al*. [57] studied the local diffusion rates of the intercalated [Na–solvent]$^+$ species in graphite by visualizing the atomic structural change of HOPG using an *in-situ* EC-STM technique. By applying an external voltage, quantitative measurement of the local topographic changes, such as the lattice expansion of a single graphene layer, could be achieved. By following the movement of the height profile, the diffusion rate of [Na–solvent]$^+$ in the graphite could be determined (Figure 4d). The diffusion rates for [Na–G$_3$]$^+$ and [Na–G$_4$]$^+$ were determined to be 5.9 and 22.1 nm s^{-1}, respectively. The fast diffusion kinetics of the intercalants should contribute to the high rate capability of graphite anodes. For largely different diffusion rates, Seidl *et al*. proposed that [Na–G$_3$]$^+$ complexes with a coordination number (CN) of 4 were under coordinated compared with those with a CN of 5 for [Na–G$_4$]$^+$. Thus, the local interaction between the Na ion and graphene layers would not be properly negated, leading to hindered diffusion of [Na–G$_3$]$^+$ in graphite. An *ab initio* molecular dynamics study also showed that the diffusivity of [Na–DEGDME]$^+$ complex in graphite is 1.1×10^{-8} cm^2 s^{-1} and that the activation barrier for diffusion is 0.13 eV, suggesting the fast kinetics of [Na–solvent]$^+$ complexes in graphite.[78]

The chemical composition and internal configuration of stage 1 [Na–DEGDME]$^+$ intercalated graphite was investigated by Kim *et al*.[54] They systematically investigated the configurations

11

of fully co-intercalated graphite by combining a suite of experimental characterization tools and density functional theory (DFT) calculations. The measured weight changes upon co-intercalation and energy-dispersive X-ray spectroscopy analysis suggested that one DEGDME molecule is intercalated with a single Na ion. Considering this information as well as the experimental capacity of electrodes and DFT calculations, they concluded that the [Na–DEGDME]$^+$ complex is doubly stacked in graphite galleries with a composition of [Na–DEGDME]C$_{21}$. This configuration contradicts that reported by Jache *et al.*, who suggested a composition of [Na(DEGDME)$_2$]C$_{20}$,[53] but is consistent with the [Na–DEGDME]C$_{20}$ configuration reported by Seidl *et al*. [57]

2.4 Advantages and challenges for co-intercalation

The discussion of the reaction processes and the electrochemical performance summarized in Table 1 reveals several unique advantages for Na co-intercalation: (i) an exceptionally high rate capability (for example, FLG electrodes maintained 65% of the maximum capacity when cycling at 30 A g^{-1}),[56] (ii) long cycle life with high coulombic efficiencies, and (iii) a stable interface.[79,80] Strong evidence of these advantages is that the reported cycle life of graphitic carbon anodes was always longer than 1000 cycles,[52,55,56,70,71,74] which is appealing for practical applications. By taking advantage of co-intercalation of graphite anodes, high power densities and long cycle life were also demonstrated in LIBs and KIBs.[81–83] For example, Kim *et al*.[83] exploited the Li–ether co-intercalation in graphite to obtain high-power LIBs. Graphite electrodes based on co-intercalation were capable of delivering a capacity retention of 87% of the theoretical capacity at a current density of 1 A g^{-1}; in contrast, a negligible capacity was achieved for conventional Li-ion intercalation at 1 A g^{-1}.

There are several practical issues that need to be addressed concerning co-intercalation in graphite. First, the electrodes typically experience large volume variations during cycles (*e.g.*, 70%−100% in Figure 4b).[77] In LIB configurations, the swelling of the external dimensions of a battery should be limited to below 5% to ensure the structural stability and safety of battery

packs.[84] The large volume changes would induce new challenges in constructing practical SIB full cells. In addition, because the solvent participates in the electrochemical reaction, large amounts of electrolyte are required for the cell configuration, offsetting the benefit of cost-effective SIBs. Second, Na co-intercalation in graphite usually delivers specific capacities of 100–150 mAh g^{-1} and average Na storage potentials of 0.6–0.8 V.[52,55,56,71,74] The specific capacities are lower and the operating potentials are higher than those for hard carbon anodes (~300 mAh g^{-1} and ~0.1 V, respectively[35,47,48]), leading to unattractive specific energy densities of graphite anodes. Future studies should aim at finding co-intercalation reactions of graphite with higher specific capacities or/and lower reaction potentials. For example, the redox potential was shown to be sensitively affected by the solvent species, which could be a viable way to optimize it.[52,54,57] Third, many issues related to the co-intercalation reaction mechanisms remain unclear, and the co-intercalation phenomenon has been only observed in specific solvents (*e.g.*, liner ethers).[85] Although Yoon *et al.* [51] attempted to explain the solvent dependency of co-intercalation phenomenon from the viewpoint of the chelate effect and the LUMO level of [Na–solvent]$^+$ complexes, additional experimental and theoretical studies are needed. In addition, Na co-intercalation in graphite was identified as a staging process in which [Na–solvent]$^+$ was first inserted in every third layer for a stage 3 Na-GIC and in every second layer for a stage 2 Na-GIC.[54] However, the phase transition from a stage 3 to a stage 2 Na-GIC can hardly be explained by the classic staging model. Although Seidl *et al.*[57] attempted to use Doumas–Herold's model[86] to explain the transition from stage 3 to stage 2 via continuous lattice filling with [Na–solvent]$^+$, neither experimental nor theoretical evidence has been reported to support this hypothesis. Moreover, few efforts have been devoted to studying the solid electrolyte interphase (SEI) layers of graphite anodes in SIBs. Contradictive statements even exist about the formation and stability of the SEI. For example, Maibach *et al.*[87] suggested that a SEI formed during initial discharge but broke and grew during the following cycles because of the large volume

13

expansion of graphite. In contrast, Goktas *et al*.[77] claimed that the formation of the SEI layer was restricted to the first cycles and that no additional side reactions occurred in the following cycles. Thus, future studies should be conducted to clarify the formation and stability of the SEI as well as the formation mechanisms and its chemical composition and morphology. Finally, studies about Na-ion full batteries with graphite anodes are still in their infancy. The full cells in literature usually exhibit low energy densities, low operating potentials (<3 V), low initial coulombic efficiencies, and insufficient life span.[52,55,70,74] More studies are needed to develop practical Na-ion full cells with Na co-intercalation graphite anodes.

3. Expanded graphite anodes

Before the realization of Na storage in natural graphite through co-intercalation reactions, expanded graphite anodes were explored. Researchers believed that the incapability of Na-ion intercalation into graphite was due to the small interlayer distance of graphite (~0.34 nm). Therefore, Cao *et al.* prepared expanded graphite to enlarge the interlayer spacing of graphite for Na insertion.[44] The expanded graphite was synthesized by oxidizing natural graphite using modified Hummer's method to decorate graphene layers with oxygenated functional groups, and then, the oxidized graphite was partially reduced to remove most of these groups but leave an enlarged interlayer spacing of ~0.43 nm (**Figure 5**a).[88] The optimal expanded graphite was capable of delivering a high Na storage capacity of ~300 mAh g^{-1} (Figure 5b). The Na storage mechanisms were claimed to be reversible insertion/extraction of Na from the expanded graphite galleries. The electrochemical response from cyclic voltammetry analyses supported the ion-diffusion-controlled reaction. Although the expanded graphite exhibited a remarkable capacity retention of ~74% after 2000 cycles (Figure 5c), the low initial coulombic efficiency (<50%) and moderate rate capacity (184 mAh g^{-1} at 0.1 A g^{-1}) still need to be addressed for practical application. Following this work, the correlation between the microstructure of expanded graphite and the electrochemical performance was investigated.

14

The role of functional groups in Na ion intercalation in expanded graphite was studied using first-principles calculations,[89] which revealed that the epoxide-rich expanded graphite exhibited much higher specific capacities than hydroxyl-rich and/or hydroxyl–epoxide mixture counterparts (Figure 5d). The higher specific capacity was attributed to the stronger Na ion binding affinity toward the epoxide group and the larger interlayer spacing of expanded graphite for the epoxide-only structure compared with those for the hydroxyl group. In addition, the Na-ion diffusion kinetics were calculated to be the highest for the epoxide-only expanded graphite because of the large interlayer spacing and few interlayer O–H hydrogen bonds. This work suggested the modification of the Na storage performance by regulating the functional groups in expanded graphite. Cabello *et al.* studied the effect of the chemical structure and morphology of expanded graphite fabricated using different methods on the Na co-intercalation properties.[72] The expanded graphite materials were prepared by (i) fast heating of graphite bisulfate or the reduction of graphite oxide using (ii) Broddie's method or (iii) Hummer's method, which resulted in an interlayer spacing/crystalline size of 3.388 Å/17.8 nm, 3.445 Å/6 nm, and 3.352 Å/8.46 nm, respectively. Sample (i) exhibited an initial coulombic efficiency of 66% and reversible capacity of 120 mAh g^{-1}, which are higher than those for natural graphite samples measured under the same conditions. The enhanced battery performance was attributed to the optimized interlayer distance by oxygen-containing groups, maximizing the possible positions for Na ion storage. The reversible capacities for samples (ii) and (iii) were lower than 60 mAh g^{-1}. This work demonstrated that the Na ion storage capacity of graphite through co-intercalation can be optimized by tailoring the interlayer spacing but that the methods used to prepare expanded graphite also play an important role in determining the Na-ion storage performance. Further research efforts are needed to elucidate the correlation between the Na storage mechanism and microstructure of expanded graphite to improve the initial coulombic efficiency and synthesize low-cost expanded graphite.

4. Graphene (oxide) anodes

4.1 Na storage mechanisms and performance in graphene (oxide) anodes

Since the first successful demonstration of single-layer graphene in 2004, graphene and graphene-based composites have attracted tremendous research and industrial interest because of their intriguing and unique electrical and mechanical properties.[90] It has been claimed that the Li storage capacity of single-layer graphene can be almost doubled compared with that of graphite through the formation of Li_2C_6 achieved by adsorbing Li ions on both sides of the graphene plane.[91] Similarly, whether single-layer graphene can also absorb Na ions on both sides is an interesting topic. To this end, single-layer graphene on copper foil was deposited using chemical vapor deposition and was subjected to cyclic voltammetry and galvanostatic cyclic tests.[92] Unfortunately, the amount of Na ions adsorbed/desorbed per surface area was low and only comparable to that for bare copper electrodes under the same conditions (**Figure 6**a), implying that the capability of pristine graphene to absorb Na ions is low, which is consistent with the aforementioned theoretical studies.[50,51,67,93,94] To increase the Na adsorption energy on graphene, structural engineering by inducing heteroatoms has been conducted. For example, "protrusions" in graphene were created by phosphorus doping.[95] Different than the "hole" defects induced by nitrogen doping, the "protrusions" not only introduced abundant Na adsorption sites but also improved the mobility of electrons and Na ions by enlarging the *d*-spacing of graphene layers (Figure 6b). As a result, phosphorus-doped graphene exhibited superior electrochemical performance with a high cyclic capacity of 374 mAh g^{-1} at 25 mA g^{-1} (Figure 6c) and excellent rate capability. Notably, *in-situ* transmission electron microscopy (TEM) revealed that Na could reversibly intercalate into the graphene layers with the interlayer spacing changing between 0.47 and 0.45 nm during discharge/charge processes (Figure 6d). Similarly, sulfur-,[96,97] boron-[98] and nitrogen-doped[99,100] graphene-based electrodes have also been reported to exhibit high specific

16

capacities and rate capabilities owing to the enriched active sites and enlarged interlayer space of graphene.

The functional groups attached to graphene play an important role in determining the Na storage mechanisms and battery performance. Reduced graphene oxide (rGO) paper prepared by vacuum filtration and annealing contained large amounts of oxygenated functional groups and had an interlayer spacing of ~0.37 nm,[101] which enabled the intercalation of Na ions within graphene layers and adsorption on the graphene surface. Tuning of the annealing temperature and atmosphere of the rGO paper greatly affected the Na storage performance. For example, the Na charge capacity was only 13 mAh g^{-1} for rGO annealed at 900 °C in Ar or at 500 °C in NH_3, whereas a larger Na storage capacity of 140 mAh g^{-1} was realized for a specimen annealed at 500 °C in Ar (Figure 6e).[102] This behavior was attributed to the decreased interlayer spacing with increasing annealing temperature in Ar and/or the eliminated oxygenated functional groups at moderate temperature in the reducing NH_3 atmosphere. This finding was also supported by another work in which holey rGO sheets annealed at 300 °C or 1100 °C exhibited cyclic capacities of 220 and 147 mAh g^{-1}, respectively [103]. However, one challenge for rGO annealed at low temperature is the poor electrical conductivity and low initial coulombic efficiency resulting from the abundant residual oxygen-containing functional groups. To achieve high conductivity without decreasing the interlayer spacing of rGO, a rapid annealing method was developed, in which the reduction occurred within minutes or even seconds.[104] The rapidly released gas during the reduction of GO prevented the stacking of GO sheets that occurred during the conventional process, ensuring the formation of monolayer rGO sheets with a large surface area exposed to Na ions. The rapidly reduced GO exhibited a high reversible capacity of 450 mAh g^{-1}, which remained ~200 mAh g^{-1} after 750 cycles. The Na storage mechanisms were also investigated using *in-situ* TEM, which revealed reversible Na metal formation on the rGO surface during charge/discharge (Figure 6f), suggesting a metal cluster formation

17

mechanism. Irreversible formation of a Na_2O SEI during the first cycle was also observed using *in-situ* TEM, providing evidence of the large capacity loss in the first cycle.

Although graphene (oxide) anodes have been shown to exhibit impressive cyclic stability and high Na storage capacities, several important problems remain. First, most of the reported rGO electrodes exhibit low initial coulombic efficiencies (even below 50%),[96–100] which is far from sufficient to meet the commercial demand for a coulombic efficiency of 90%. The unsatisfactory initial coulombic efficiency is mainly attributed to the formation of a thick SEI layer due to inevitable decomposition of the electrolyte and the irreversible reaction between the Na ions and oxygenated functional groups on rGO sheets.[104] More efforts such as surface modification or pre-sodiation are needed to mitigate this issue. Second, the Na storage mechanisms for rGO remain elusive. For example, graphene sheets deposited on copper foil exhibited low Na adsorption capacity on the surface[92] because of the energetically unfavorable formation of Na-GICs. In contrast, rapidly reduced GO sheets showed reversible Na metal formation on the surface with a capacity of 450 mAh g^{-1}.[104] The structural difference between graphene and rapidly annealed rGO may result in significantly different battery performance, which requires further studies to provide a clearer understanding. Third, most of the reported rGO electrodes exhibit capacities near 200 mAh g^{-1} and a slopy shape of the discharge/charge profiles without a well-defined Na storage plateau,[105,106] which signify the low energy densities of Na-ion full batteries. Strategies to improve the energy density of graphene-based electrodes in SIBs should thus be considered.

4.2 Graphene-based composite anodes

Because of its high electrical conductivity and mechanical flexibility, graphene has been widely used as a scaffold to support other active particles undergoing alloying/conversion reactions (*e.g.*, Sn, SnO_2 an Ge),[107,108] intercalation reactions (*e.g.*, TiO_2),[109] and redox reactions (*e.g.*, organic materials).[49,110] Metallic Sn is a popular alloying anode for SIBs with a high theoretical capacity of 847 mAh g^{-1} achieved by forming $Na_{3.75}Sn$ composition. The

main obstacle to the use of Sn is the large volume expansion that occurs during sodiation (~420%), which induces pulverization of the active materials and poor cyclic stability. Sn nanoparticles were uniformly deposited on a rGO scaffold, which not only facilitated the electron transport to individual Sn nanoparticles but also effectively accommodated the volume expansion during sodiation (**Figure 7**a and b).[111] The Sn/rGO electrode delivered a reversible capacity of 615 mAh g^{-1} and better capacity retention than its bare Sn counterpart (Figure 7c). Other alloying materials such as SnO_2,[107] phosphorene,[112] and Ge[108] have also been successfully hybridized with rGO to achieve enhanced cyclic capacities. Anatase TiO_2 is known to be an intercalation material but exhibits apparent pseudocapacitive performance after the first cycle because of the irreversible amorphization of TiO_2 crystals during the sodiation process.[42] The poor conductivity and sluggish ion diffusion in TiO_2 are considered the main issues retarding its Na storage kinetics. To enhance the rate capability, chemically bonded sandwich-like graphene–TiO_2 composites were prepared (Figure 7d), which exhibited high rate capabilities of 265 and 90 mAh g^{-1} at 50 and 12,000 mA g^{-1} (Figure 7e), respectively.[113] The integrated graphene and TiO_2 interface in the hybrid structure provided a feasible pathway for Na ion diffusion and prompted the intercalation pseudocapacitive behavior of Na ions in the graphene–TiO_2 electrode (Figure 7f).

Recently, increasing attention has been paid to organic electrode materials because of their abundance, environmental friendliness, and sustainability.[110] Quinones, representative organic anodes for SIBs, can deliver high Na storage capacity but suffer from serious dissolution in aprotic electrolyte, causing a shuttling effect during cycles. The use of the strong π–π interactions between graphene and conjugated organic materials has been demonstrated to be effective in simultaneously alleviating the dissolution issue and enhancing the electrical conductivity.[110] One representative example is the fabrication of Juglone/rGO composite using a self-assembly method (Figure 7g–i).[114] The strong non-covalent immobilization of the Juglone molecules via π–π interactions on the graphene scaffold yielded

a high capacity retention of 280 mAh g^{-1} after 100 cycles. This work suggests the application of graphene in mitigating the dissolution issues of organic electrode materials by chemical anchoring.

5. Conclusion and perspectives

Driven by the limited lithium resources and ever-growing demand for efficient ESSs, the number of studies on SIBs has increased dramatically in recent years. Among the large number of potentially suitable electrode materials, graphitic carbon has attracted increasing research attention because of its natural abundance, industrial feasibility, and well-established success in LIBs. Some important achievements have been demonstrated that graphitic carbon could become a promising candidate anode for SIBs. Specifically, solvated Na ions can be inserted into graphite through co-intercalation reactions with remarkable cyclic stability and power capability, expanded graphite enables Na-ion intercalation as a result of the larger interlayer spacing and functional groups, and graphene (oxide) composites with various microstructures and chemical composites can deliver high Na storage capacity via adsorption, interaction, or/and alloying/conversion reactions. The electrochemical performances of representative graphitic carbon materials for SIBs are summarized in Table 1. Several important conclusions can be extracted from the battery performances: (i) Graphitic carbon anodes can exhibit impressive long-term cyclic stability and high power capability. For example, few-layered graphene undergoing co-intercalation delivered a cyclic capacity of ~115 mAh g^{-1} at 12 A g^{-1} after 8000 cycles and a rate capacity of 100 mAh g^{-1} at 30 A g^{-1},[56] thereby far outperforming the performance of alloying/conversion anodes.[7] This excellent battery performance can be attributed to the intrinsic rapid reaction kinetics and stable structure for graphite during co-intercalation. (ii) The Na storage capacity is closely related to the microstructure and Na storage mechanisms of graphitic carbon. The reversible capacities of pure graphitic carbon lie between 100 and 300 mAh g^{-1}, whereas heteroatom-doped carbon

20

and graphene-based composites can exhibit capacities between 400 and 1000 mAh g^{-1}. Thus, the specific capacities of graphitic carbon can be improved by introducing more active sites (*e.g.*, through N-, S-, and P-doping) and active particles. (iii) The initial coulombic efficiencies (ICEs) of graphite, expanded graphite, and graphene (oxide) electrodes are mainly distributed around 70%, 50%, and less than 50% (Table 1). Apparently, all of the ICEs are far below the commercial requirement of ~90%. In addition, the ICEs decreased with increasing oxidization degree or increasing number of defects for graphitic carbon, which favors the formation of a thick SEI and induces more irreversible Na ions. Surface modification of graphitic-carbon-based electrodes or the exploration of new components for the electrolyte can be effective in improving the ICEs.

Based on the progress and potential challenges summarized in this review, we propose the following suggestions for the future development of SIBs using graphitic carbon materials.

Exploring reliable electrolytes. Electrolytes are essential for the co-intercalation and significantly affect the electrochemical properties.[115] As discussed in Section 2, ether-based electrolytes have been most widely adopted for the co-intercalation; however, further development of the electrolyte is required. Although ether-based electrolytes have been shown to possess higher ionic conductivity, better wettability with electrodes, and lower electrolyte/electrolyte interfacial resistance, they typically exhibit relatively low oxidation potentials and low boiling points (*e.g.*, 84 °C for DME and 162 °C for DEGDME *vs.* 250 °C for EC/PC),[42] which would lead to safety issues for full Na-ion battery applications. With respect to the co-intercalation of Na and ether solvent in graphite, the large ether molecules lead to high operating potential and low charge capacities, eventually resulting in unsatisfactory energy densities for graphite anodes. Considering both the advantages and challenges, the community can further improve the performance of batteries in ether-based electrolytes by further investigating the components of this type of electrolyte.

21

Increasing the initial coulombic efficiency. The ICEs of reported graphitic carbon anodes remain unsatisfactory, and increasing the ICE without compromising the cyclic stability and high rate capacities remains a challenging issue. Generally, low ICEs are attributed to (i) the formation of an excess amount of the SEI layer and (ii) irreversible Na ion storage in graphitic carbon materials. For carbon anodes in SIBs, the former is generally related to the electrolyte and carbon surface chemistry, whereas the latter is closely tied to the carbon structure. Strategies proposed to alleviate these problems mainly include designing smart carbon structures, optimizing the surface functional groups, and controlling the electrolyte components. For instance, S-doped carbon sheets exhibited a much lower surface area of 39.8 $m^2 \, g^{-1}$ compared with that of 139.7 $m^2 \, g^{-1}$ for N-doped carbon, which led to a higher ICE for the S-doped carbon sheet.[96] Decreasing surface area may induce the loss of active sites and Na storage capacities of carbons, which should be considered for further optimization. In addition, modifying the electrolyte chemistry can play an important role in improving the first cycle efficiency. It was reported that the ICEs for rGO, activated carbon, and CMK-3 electrodes were improved from 39%, 13.7%, and 23.1% to 74.6%, 59.6%, and 62.8%, respectively, by replacing carbonate-based electrolytes with ether-based electrolytes.[116] The proposed reason was that the SEI layer formed in the ether-based electrolyte mainly consists of compacted, thin, and highly ionic conductive organic layers at the exterior, whereas the SEI formed in the carbonate-based electrolyte mainly consists of a thick and non-uniform mixture of organic/inorganic layers.[42]

Developing Na-ion full batteries with high energy density. Despite the superior cyclic capacity and good rate capability achieved using graphitic carbon anodes, Na-ion full batteries with high energy densities and long cycle life have not been developed, which is associated with the low operating potentials (< 3 V), unstable electrolyte/electrode interface, and high irreversible capacities at the first cycle.[117] An early graphitic-carbon-based Na-ion full cell was reported by Chen's group,[70] who fabricated graphite//$Na_3V_2(PO_4)_3$ full cells cycled in an

ether-based electrolyte. Although the graphite//$Na_3V_2(PO_4)_3$ full cell exhibited a high capacity retention of 80% after 400 cycles, the average output voltage was only 2.2 V (vs. Na^+/Na), which is much lower than that for practical LIBs. Kang's group reported graphite//$Na_{1.5}VPO_{4.8}F_{0.7}$ full cells[52] with a high average voltage of 2.92 V and energy density of ~120 Wh kg^{-1}. However, the capacity retention was only 70% after 250 cycles at 0.5 A g^{-1}, which may be attributed to the high cutoff voltage of 4.2 V inducing decomposition of the ether-based electrolyte during charging. Other graphitic-carbon-based full cells, such as graphite//Al_2O_3@$Na_3V_2(PO_4)_3$,[118] porous graphite//$Na_3V_2(PO_4)_3$,[119] carbon nanotube@carbon black//$Na_{3.12}Fe_{2.44}(P_2O_7)_2$,[120] and multi-walled carbon nanotube @graphite oxide nanoribbon//Na_xMnO_2[121] have also been reported. However, none of these full cells exhibited output voltages above 3 V and a cyclic life beyond 1000 cycles, indicating that great efforts are needed to develop advanced Na-ion full cells. In addition, the safety, manufacturing cost, and feasibility of the materials should also be considered for further development of SIBs.

Reference

[1]   M. Armand, J.M. Tarascon, *Nature* **2008**, *451*, 652.

[2]   D. Larcher, J.M. Tarascon, *Nat. Chem.* **2015**, *7*, 19.

[3]   Z. L. Xu, X. Liu, Y. Luo, L. Zhou, J. K. Kim, *Prog. Mater. Sci.* **2017**, *90*, 1.

[4]   Z. L. Xu, J. K. Kim, K. Kang, *Nano Today* **2018**, *19*, 84.

[5]   S. W. Kim, D. H. Seo, X. Ma, G. Ceder, K. Kang, *Adv. Energy Mater.* **2012**, *2*, 710.

[6]   H. Pan, Y.S. Hu, L. Chen, *Energy Environ. Sci.* **2013**, *6*, 2338.

[7]   H. Kim, H. Kim, Z. Ding, M. H. Lee, K. Lim, G. Yoon, K. Kang, *Adv. Energy Mater.* **2016**, *6*, 1600943.

[8]   B. W. Jaskula, *Miner. Commod. Summ. 2018* **2018**, 98.

[9]   J.Y. Hwang, S.T. Myung, Y.K. Sun, *Chem. Soc. Rev.* **2017**, *46*, 3529.

[10]   Fox-Davies resouce specialist, The Lithium Market, in *http://doc.xueqiu.com/1497add8471193fc2e583642.pdf* Accessed: June, 2018.

[11]   H. Vikström, S. Davidsson, M. Höök, *Appl. Energy* **2013**, *110*, 252.

[12]   M. S. Whittingham, *Prog. Solid State Chem.* **1978**, *12*, 41.

[13]   A. S. Nagelberg, W. L. Worrell, *J. Solid State Chem.* **1979**, *29*, 345.

[14]   Z. L. Xu, S. Yao, J. Cui, L. Zhou, J. K. Kim, *Energy Storage Mater.* **2017**, *8*, 10.

[15]   W.J. Li, C. Han, W. Wang, F. Gebert, S.L. Chou, H.K. Liu, X. Zhang, S.X. Dou, *Adv. Energy Mater.* **2017**, *7*, 1700274.

[16]   Y. You, A. Manthiram, *Adv. Energy Mater.* **2018**, *8*, 1701785.

[17]   J. Kim, H. Kim, K. Kang, *Adv. Energy Mater.* **2018**, *8*, 1702646.

[18]   X. Xiang, K. Zhang, J. Chen, *Adv. Mater.* **2015**, *27*, 5343.

[19]   P. Vassilaras, X. Ma, X. Li, G. Ceder, *J. Electrochem. Soc.* **2012**, *160*, A207.

[20]   N. Yabuuchi, M. Kajiyama, J. Iwatate, H. Nishikawa, S. Hitomi, R. Okuyama, R. Usui, Y. Yamada, S. Komaba, *Nat. Mater.* **2012**, *11*, 512.

[21]   L. Liu, X. Li, S.-H. Bo, Y. Wang, H. Chen, N. Twu, D. Wu, G. Ceder, *Adv. Energy Mater.* **2015**, *5*, 1500944.

[22]   R. A. Shakoor, D.-H. Seo, H. Kim, Y.-U. Park, J. Kim, S.-W. Kim, H. Gwon, S. Lee, K. Kang, *J. Mater. Chem.* **2012**, *22*, 20535.

[23]   H. Kim, I. Park, D. H. Seo, S. Lee, S. W. Kim, W. J. Kwon, Y. U. Park, C. S. Kim, S. Jeon, K. Kang, *J. Am. Chem. Soc.* **2012**, *134*, 10369.

[24] Y. U. Park, D. H. Seo, H. S. Kwon, B. Kim, J. Kim, H. Kim, I. Kim, H. I. Yoo, K. Kang, *J. Am. Chem. Soc.* **2013**, *135*, 13870.

[25] R. Tripathi, S. M. Wood, M. S. Islam, L. F. Nazar, *Energy Environ. Sci.* **2013**, *6*, 2257.

[26] Y. U. Park, D. H. Seo, H. Kim, J. Kim, S. Lee, B. Kim, K. Kang, *Adv. Funct. Mater.* **2014**, *24*, 4603.

[27] K. Chihara, N. Chujo, A. Kitajou, S. Okada, *Electrochim. Acta* **2013**, *110*, 240.

[28] S. Wang, L. Wang, Z. Zhu, Z. Hu, Q. Zhao, J. Chen, *Angew. Chemie* **2014**, *126*, 6002.

[29] H. Kim, J. E. Kwon, B. Lee, J. Hong, M. Lee, S. Y. Park, K. Kang, *Chem. Mater.* **2015**, *27*, 7258.

[30] Y. Lu, L. Wang, J. Cheng, J. B. Goodenough, *Chem. Commun.* **2012**, *48*, 6544.

[31] L. Wang, J. Song, R. Qiao, L. A. Wray, M. A. Hossain, Y. De Chuang, W. Yang, Y. Lu, D. Evans, J. J. Lee, S. Vail, X. Zhao, M. Nishijima, S. Kakimoto, J. B. Goodenough, *J. Am. Chem. Soc.* **2015**, *137*, 2548.

[32] J. Song, L. Wang, Y. Lu, J. Liu, B. Guo, P. Xiao, J. J. Lee, X. Q. Yang, G. Henkelman, J. B. Goodenough, *J. Am. Chem. Soc.* **2015**, *137*, 2658.

[33] M. M. Doeff, M. M. Doeff, Y. Ma, Y. Ma, S. J. Visco, S. J. Visco, L. C. De Jonghe, L. C. De Jonghe, *J. Electrochem. Soc.* **1993**, *140*, 169.

[34] P. Thomas, J. Ghanbaja, D. Billaud, *Electrochim. Acta* **1999**, *45*, 423.

[35] D. A. Stevens, J. R. Dahn, *J. Electrochem. Soc.* **2000**, *147*, 1271.

[36] D. A. Stevens, J. R. Dahn, *J. Electrochem. Soc.* **2001**, *148*, A803.

[37] J. Cui, Z.L. Xu, S. Yao, J. Huang, J.Q. Huang, S. Abouali, M. A. Garakani, X. Ning, J.K. Kim, *J. Mater. Chem. A* **2016**, *4*, 10964.

[38] S. Yao, J. Cui, Z. Lu, Z.L. Xu, L. Qin, J. Huang, Z. Sadighi, F. Ciucci, J.K. Kim, *Adv. Energy Mater.* **2017**, *7*, 1602149.

[39] Y. Kim, Y. Park, A. Choi, N. S. Choi, J. Kim, J. Lee, J. H. Ryu, S. M. Oh, K. T. Lee, *Adv. Mater.* **2013**, *25*, 3045.

[40]   C. Wang, L. Wang, F. Li, F. Cheng, J. Chen, *Adv. Mater.* **2017**, *29*, 1702212.

[41]   J. Qian, X. Wu, Y. Cao, X. Ai, H. Yang, *Angew. Chem - Int. Ed.* **2013**, *52*, 4633.

[42]   Z.L. Xu, K. Lim, K.Y. Park, G. Yoon, W. M. Seong, K. Kang, *Adv. Funct. Mater.* **2018**, *8*, 1802099.

[43]   Y. Zhang, P. Zhu, L. Huang, J. Xie, S. Zhang, G. Cao, X. Zhao, *Adv. Funct. Mater.* **2015**, *25*, 481.

[44]   Y. Cao, L. Xiao, M. L. Sushko, W. Wang, B. Schwenzer, J. Xiao, Z. Nie, L. V. Saraf, Z. Yang, J. Liu, *Nano Lett.* **2012**, *12*, 3783.

[45]   J. Ding, H. Wang, Z. Li, A. Kohandehghan, K. Cui, Z. Xu, B. Zahiri, X. Tan, E. M. Lotfabad, B. C. Olsen, D. Mitlin, *ACS Nano* **2013**, *7*, 11004.

[46]   M. S. Balogun, Y. Luo, W. Qiu, P. Liu, Y. Tong, *Carbon* **2016**, *98*, 162.

[47]   H. Hou, X. Qiu, W. Wei, Y. Zhang, X. Ji, *Adv. Energy Mater.* **2017**, *7*, 1602898.

[48]   D. Saurel, B. Orayech, B. Xiao, D. Carriazo, X. Li, T. Rojo, *Adv. Energy Mater.* **2018**, *8*, 1703268.

[49]   Y. Lu, Y. Lu, Z. Niu, J. Chen, *Adv. Energy Mater.* **2018**, *4*, 1702469.

[50]   Y. Liu, B. V. Merinov, W. A. Goddard, *Proc. Natl. Acad. Sci.* **2016**, *113*, 3735.

[51]   G. Yoon, H. Kim, I. Park, K. Kang, *Adv. Energy Mater.* **2017**, *7*, 1601519.

[52]   H. Kim, J. Hong, Y. U. Park, J. Kim, I. Hwang, K. Kang, *Adv. Funct. Mater.* **2015**, *25*, 534.

[53]   B. Jache, P. Adelhelm, *Angew. Chem- Int. Ed.* **2014**, *53*, 10169.

[54]   H. Kim, J. Hong, G. Yoon, H. Kim, K.Y. Park, M.S. Park, W.S. Yoon, K. Kang, *Energy Environ. Sci.* **2015**, *8*, 2963.

[55]   I. Hasa, X. Dou, D. Buchholz, Y. Shao-Horn, J. Hassoun, S. Passerini, B. Scrosati, *J. Power Sources* **2016**, *310*, 26.

[56]   A. P. Cohn, K. Share, R. Carter, L. Oakes, C. L. Pint, *Nano Lett.* **2016**, *16*, 543.

[57]   L. Seidl, N. Bucher, E. Chu, S. Hartung, S. Martens, O. Schneider, U. Stimming,

Energy Environ. Sci. **2017**, *10*, 1631.

[58] D. Aurbach, Y. Ein-Eli, *J. Electrochem. Soc* **1995**, *16*, 209.

[59] V. Etacheri, R. Marom, R. Elazari, G. Salitra, D. Aurbach, *Energy Environ. Sci.* **2011**, *4*, 3243.

[60] Z. Jian, W. Luo, X. Ji, *J. Am. Chem. Soc.* **2015**, *137*, 11566.

[61] J. O. Besenhard, *Carbon* **1976**, *14*, 111.

[62] M. S. Dresselhaus, G. Dresselhaus, *Adv. Phys.* **2002**, *51*, 1.

[63] P. Ge, M. Fouletier, *Solid State Ionics* **1988**, *28–30*, 1172.

[64] R. C. Asher, S. A. Wilson, *Nature* **1958**, *181*, 409.

[65] D. P. Divincenzo, E. J. Mele, *Phys. Rev. B* **1985**, *32*, 2538.

[66] K. Nobuhara, H. Nakayama, M. Nose, S. Nakanishi, H. Iba, *J. Power Sources* **2013**, *243*, 585.

[67] Z. Wang, S. M. Selbach, T. Grande, *RSC Adv.* **2014**, *4*, 4069.

[68] Y. Okamoto, *J. Phys. Chem. C* **2014**, *118*, 16.

[69] H. Moriwake, A. Kuwabara, C. A. J. Fisher, Y. Ikuhara, *RSC Adv.* **2017**, *7*, 36550.

[70] Z. Zhu, F. Cheng, Z. Hu, Z. Niu, J. Chen, *J. Power Sources* **2015**, *293*, 626.

[71] W. Xiao, Q. Sun, J. Liu, B. Xiao, P. A. Glans, J. Li, R. Li, J. Guo, W. Yang, T. K. Sham, X. Sun, *Nano Res.* **2017**, *10*, 4378.

[72] M. Cabello, X. Bai, T. Chyrka, G. F. Ortiz, P. Lavela, R. Alcántara, J. L. Tirado, *J. Electrochem. Soc.* **2017**, *164*, A3804.

[73] Y.E. Zhu, L. Yang, X. Zhou, F. Li, J. Wei, Z. Zhou, *J. Mater. Chem. A* **2017**, *5*, 9528.

[74] P. Han, X. Han, J. Yao, L. Zhang, X. Cao, C. Huang, G. Cui, *J. Power Sources* **2015**, *297*, 457.

[75] A. N. Dey, B. P. Sullivan, *J. Electrochem. Soc.* **1970**, *117*, 222.

[76] T. Abe, N. Kawabata, Y. Mizutani, M. Inaba, Z. Ogumi, *J. Electrochem. Soc.* **2003**, *150*, A257.

[77] M. Goktas, C. Bolli, E. J. Berg, P. Novák, K. Pollok, F. Langenhorst, M. v. Roeder, O. Lenchuk, D. Mollenhauer, P. Adelhelm, *Adv. Energy Mater.* **2018**, DOI 10.1002/aenm.201702724.

[78] S. C. Jung, Y. J. Kang, Y. K. Han, *Nano Energy* **2017**, *34*, 456.

[79] W. Luo, F. Shen, C. Bommier, H. Zhu, X. Ji, L. Hu, *Acc. Chem. Res.* **2016**, *49*, 231.

[80] M. Lao, Y. Zhang, W. Luo, Q. Yan, W. Sun, S. X. Dou, *Adv. Mater.* **2017**, *29*, 1700622.

[81] H. Kim, G. Yoon, K. Lim, K. Kang, *Chem. Commun.* **2016**, *52*, 12618.

[82] A. P. Cohn, N. Muralidharan, R. Carter, K. Share, L. Oakes, C. L. Pint, *J. Mater. Chem. A* **2016**, *4*, 14954.

[83] H. Kim, K. Lim, G. Yoon, J.H. Park, K. Ku, H.D. Lim, Y.E. Sung, K. Kang, *Adv. Energy Mater.* **2017**, *7*, 1700418.

[84] R. Dash, S. Pannala, *Mater. Today* **2016**, *19*, 483.

[85] B. Jache, J. O. Binder, T. Abe, P. Adelhelm, *Phys. Chem. Chem. Phys.* **2016**, *18*, 14299.

[86] N. Daumas, A. Herold, *C.R. Seances Acad. Sci., Ser. C* **1969**, *268*, 273.

[87] J. Maibach, F. Jeschull, D. Brandell, K. Edström, M. Valvo, *ACS Appl. Mater. Interfaces* **2017**, *9*, 12373.

[88] Y. Wen, K. He, Y. Zhu, F. Han, Y. Xu, I. Matsuda, Y. Ishii, J. Cumings, C. Wang, *Nat. Commun.* **2014**, *5*, 4033.

[89] Y.J. Kang, S. C. Jung, J. W. Choi, Y.K. Han, *Chem. Mater.* **2015**, *27*, 5402.

[90] Q. Li, N. Mahmood, J. Zhu, Y. Hou, S. Sun, *Nano Today* **2014**, *9*, 668.

[91] E. J. Yoo, J. Kim, E. Hosono, H. S. Zhou, T. Kudo, I. Honma, *Nano Lett.* **2008**, *8*, 2277.

[92] A. Ramos, I. Cameán, N. Cuesta, A. B. García, *Electrochim. Acta* **2015**, *178*, 392.

[93] L.H. Yao, M.S. Cao, H.J. Yang, X.J. Liu, X.Y. Fang, J. Yuan, *Comput. Mater. Sci.* **2014**, *85*, 179.

[94] S. Yang, S. Li, S. Tang, W. Dong, W. Sun, D. Shen, M. Wang, *Theor. Chem. Acc.*

2016, *135*, 164.

[95] Y. Yang, D.M. Tang, C. Zhang, Y. Zhang, Q. Liang, S. Chen, Q. Weng, M. Zhou, Y. Xue, J. Liu, J. Wu, Q. H. Cui, C. Lian, G. Hou, F. Yuan, Y. Bando, D. Golberg, X. Wang, *Energy Environ. Sci.* **2017**, *10*, 979.

[96] L. Qie, W. Chen, X. Xiong, C. Hu, F. Zou, P. Hu, Y. Huang, *Adv. Sci.* **2015**, *2*, 1500195.

[97] M. M. Islam, C. M. Subramaniyam, T. Akhter, S. N. Faisal, A. I. Minett, H. K. Liu, K. Konstantinov, S. X. Dou, *J. Mater. Chem. A* **2017**, *5*, 5290.

[98] Y. Wang, C. Wang, Y. Wang, H. Liu, Z. Huang, *ACS Appl. Mater. Interfaces* **2016**, *8*, 18860.

[99] J. Xu, M. Wang, N. P. Wickramaratne, M. Jaroniec, S. Dou, L. Dai, *Adv. Mater.* **2015**, *27*, 2042.

[100] Y. Ma, Q. Guo, M. Yang, Y. Wang, T. Chen, Q. Chen, X. Zhu, Q. Xia, S. Li, H. Xia, *Energy Storage Mater.* **2018**, *13*, 134.

[101] Y. X. Wang, S. L. Chou, H. K. Liu, S. X. Dou, *Carbon N. Y.* **2013**, *57*, 202.

[102] L. David, G. Singh, *J. Phys. Chem. C* **2014**, *118*, 28401.

[103] X.F. Luo, C.H. Yang, J.K. Chang, *J. Mater. Chem. A* **2015**, *3*, 17282.

[104] J. Wan, F. Shen, W. Luo, L. Zhou, J. Dai, X. Han, W. Bao, Y. Xu, J. Panagiotopoulos, X. Fan, D. Urban, A. Nie, R. Shahbazian-Yassar, L. Hu, *Chem. Mater.* **2016**, *28*, 6528.

[105] Y. S. Yun, Y. U. Park, S. J. Chang, B. H. Kim, J. Choi, J. Wang, D. Zhang, P. V. Braun, H. J. Jin, K. Kang, *Carbon N. Y.* **2016**, *99*, 658.

[106] X.F. Luo, C.H. Yang, Y.Y. Peng, N.W. Pu, M.D. Ger, C.T. Hsieh, J.-K. Chang, *J. Mater. Chem. A* **2015**, *3*, 10320.

[107] D. Su, H.-J. Ahn, G. Wang, *Chem. Commun.* **2013**, *49*, 3131.

[108] X. Wang, L. Fan, D. Gong, J. Zhu, Q. Zhang, B. Lu, *Adv. Funct. Mater.* **2016**, *26*, 1104.

[109] S. K. Das, B. Jache, H. Lahon, C. L. Bender, J. Janek, P. Adelhelm, *Chem. Commun.*

2016, *52*, 1428.

[110] S. Lee, G. Kwon, K. Ku, K. Yoon, S.K. Jung, H.D. Lim, K. Kang, *Adv. Mater.* **2018**, *3*, 1704682.

[111] Y. Jeon, X. Han, K. Fu, J. Dai, J. H. Kim, L. Hu, T. Song, U. Paik, *J. Mater. Chem. A* **2016**, *4*, 18306.

[112] J. Sun, H. W. Lee, M. Pasta, H. Yuan, G. Zheng, Y. Sun, Y. Li, Y. Cui, *Nat. Nanotechnol.* **2015**, *10*, 980.

[113] C. Chen, Y. Wen, X. Hu, X. Ji, M. Yan, L. Mai, P. Hu, B. Shan, Y. Huang, *Nat. Commun.* **2015**, *6*, 6929.

[114] H. Wang, P. Hu, J. Yang, G. Gong, L. Guo, X. Chen, *Adv. Mater.* **2015**, *27*, 2348.

[115] H. Che, S. Chen, Y. Xie, H. Wang, K. Amine, X.Z. Liao, Z.F. Ma, *Energy Environ. Sci.* **2017**, *10*, 1075.

[116] J. Zhang, D.W. Wang, W. Lv, S. Zhang, Q. Liang, D. Zheng, F. Kang, Q.-H. Yang, *Energy Environ. Sci.* **2017**, *10*, 370.

[117] J. Deng, W.B. Luo, S.L. Chou, H.K. Liu, S.X. Dou, *Adv. Energy Mater.* **2018**, *8*, 1701428.

[118] R. Klee, M. Wiatrowski, M. J. Aragón, P. Lavela, G. F. Ortiz, R. Alcántara, J. L. Tirado, *ACS Appl. Mater. Interfaces* **2017**, *9*, 1471.

[119] P. Han, X. Han, J. Yao, Z. Liu, X. Cao, G. Cui, *Electrochem. commun.* **2015**, *61*, 84.

[120] Y. Niu, M. Xu, C. Cheng, S. Bao, J. Hou, S. Liu, F. Yi, H. He, C. M. Li, *J. Mater. Chem. A* **2015**, *3*, 17224.

[121] H.-Y. Chen, N. Bucher, S. Hartung, L. Li, J. Friedl, H.P. Liou, C.L. Sun, U. Stimming, M. Srinivasan, *Adv. Mater. Interfaces* **2016**, *3*, 1600357.
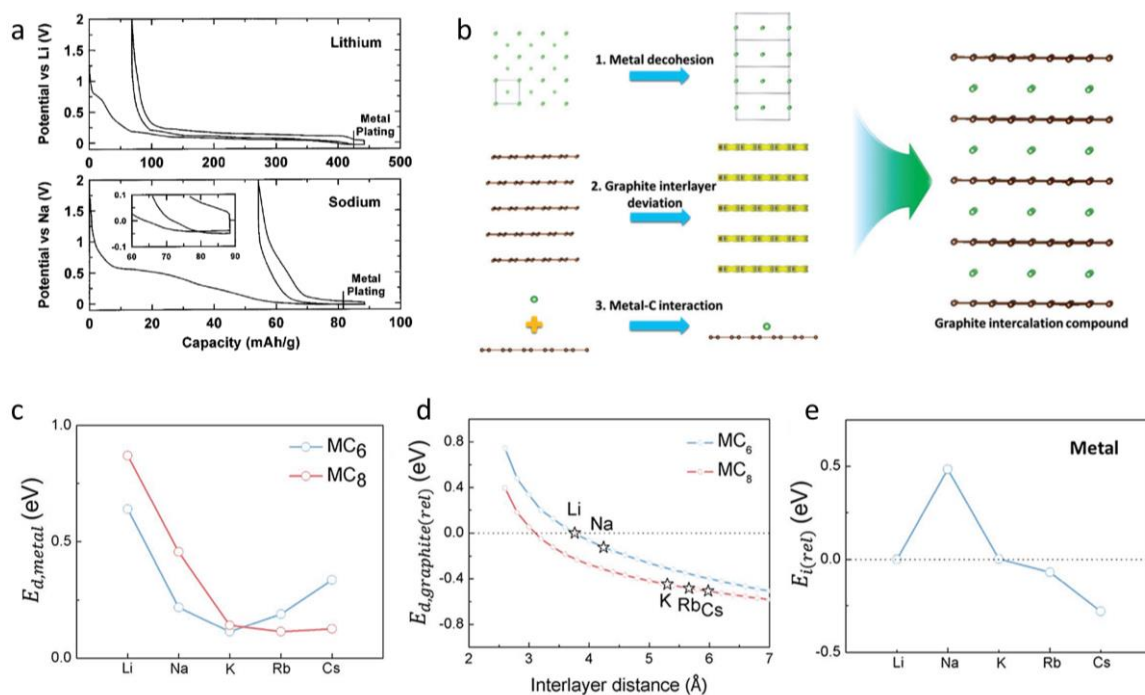
Figure 1. (a) Comparison of Li and Na intercalation in graphite,[36] (b) schematic illustration of possible major factors affecting the Na interaction in graphite, including (i) metal decohesion, (ii) graphite layer deviation and (iii) metal-C interaction, (c) $E_{d, metal}$ values upon lattice reconstruction from metal to MC_6 or MC_8 (for factor i), (d) $E_{d, graphite}$ changes upon AM intercalation and charge transfer (for factor ii) and (e) E_i between AM and a single layer graphene (for factor iii).[51] (a) Reproduced with permission.[36] Copyright 2001, Electrochemical Society. (b-e) Reproduced with permission.[51] Copyright 2017, Wiley-VCH.

31
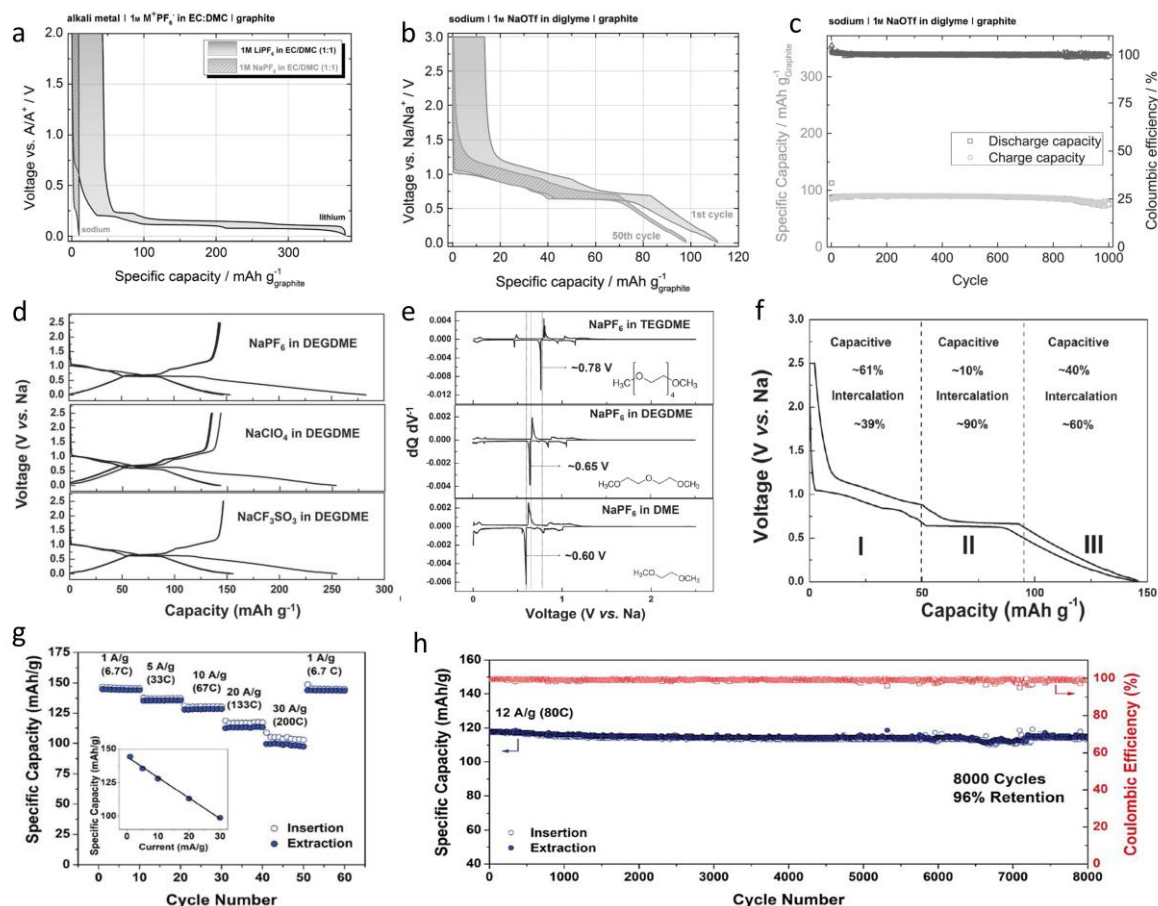
Figure 2. Comparison of discharge/charge profiles of graphite in (a) carbonate-based electrolyte and (b) ether-based electrolyte in LIBs and SIBs, (c) cycle stability of graphite in SIBs with cointercalation reactions;[53] (d) galvanostatic charge/discharge profiles with different Na salts, (e) dQ/dV of graphite-based half cells with NaPF$_6$ electrolytes in different linear ethers, (f) quantitative contributions of capacitive and intercalation to Na storage at various stages;[52] (g) high rate capability and (h) long cycle life of FLG electrodes.[56] (a-c) Reproduced with permission.[53] Copyright 2014, Wiley-VCH. (d-f) Reproduced with permission.[52] Copyright 2015, Wiley-VCH. (g, h) Reproduced with permission.[56] Copyright 2016, American Chemical Society.
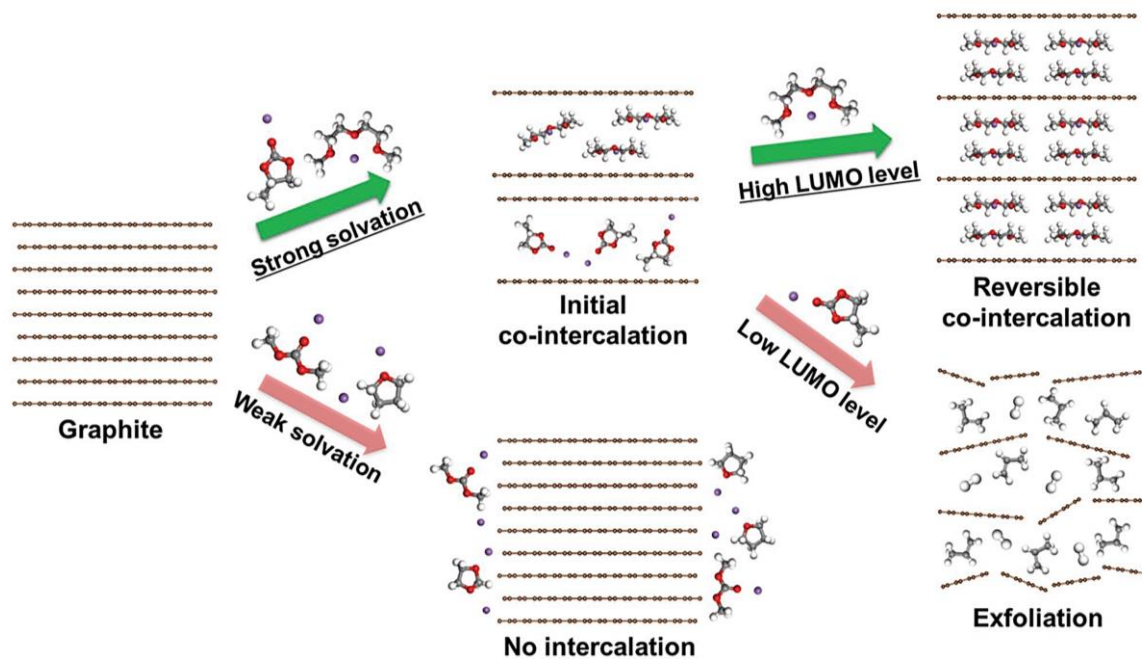
Figure 3. Schematic illustration of the conditions to realize Na cointercalation in graphite.[51] Reproduced with permission.[51] Copyright 2017, Wiley-VCH.
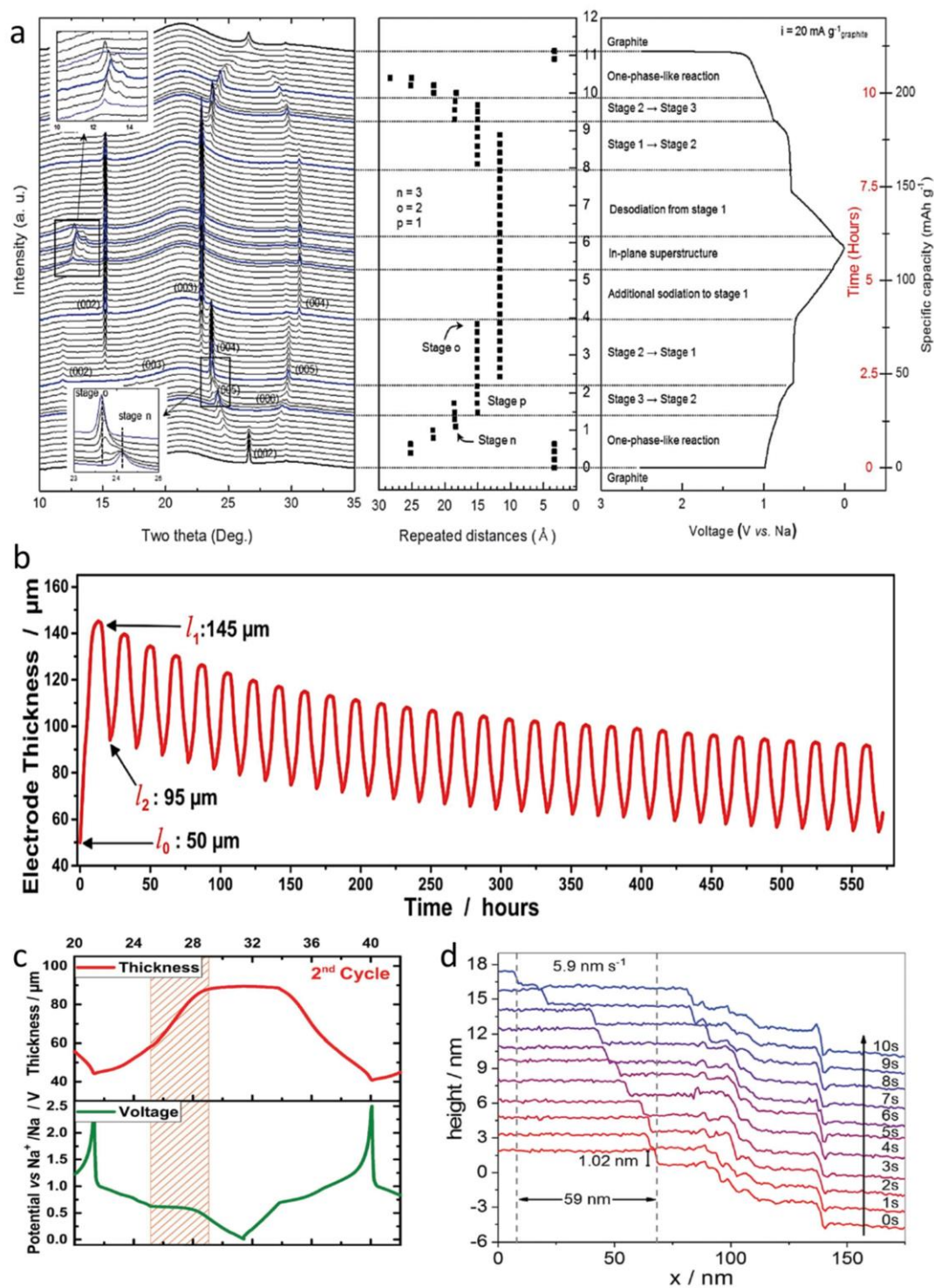
Figure 4. (a) In operando synchrotron XRD analysis of the structural evolution of graphite during electrochemical solvated-Na-ion intercalation and deintercalation reactions;[54] *in-situ* ECD analysis of the thickness changes of graphite electrodes during (b) many cycles and (c) one cycle;[77] (d) *in-situ* EC-STM analysis of the temporal propagation of graphite lattice expansion to estimate the $[Na-G_3]^+$ diffusion rate in graphite.[57] (a) Reproduced with permission.[54] Copyright 2015, Royal Society of Chemistry. (b and c) Reproduced with permission.[77] Copyright 2018, Wiley-VCH. (d) Reproduced with permission.[57] Copyright 2017, Royal Society of Chemistry.
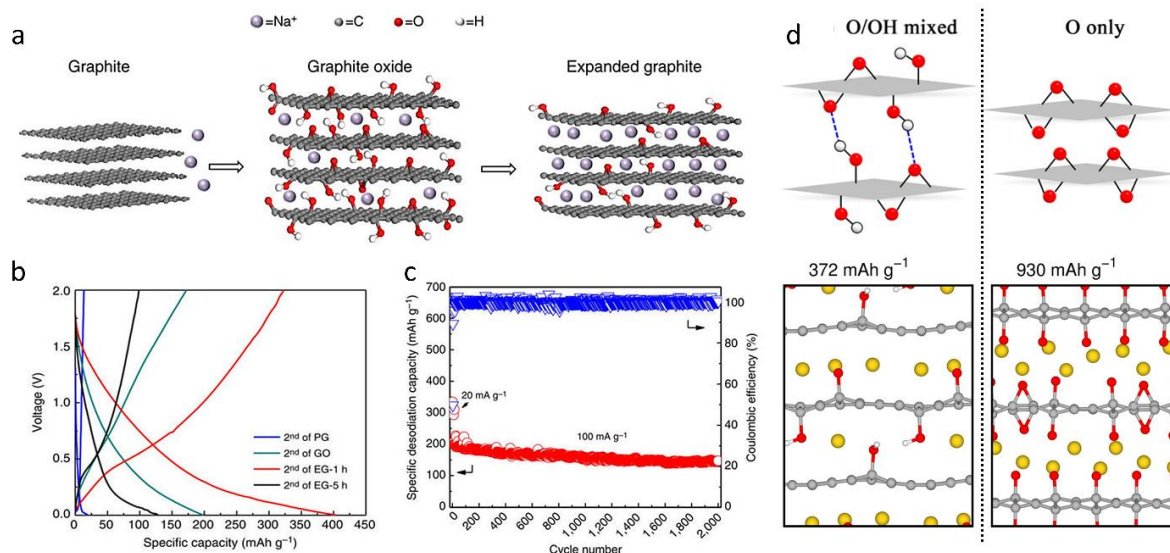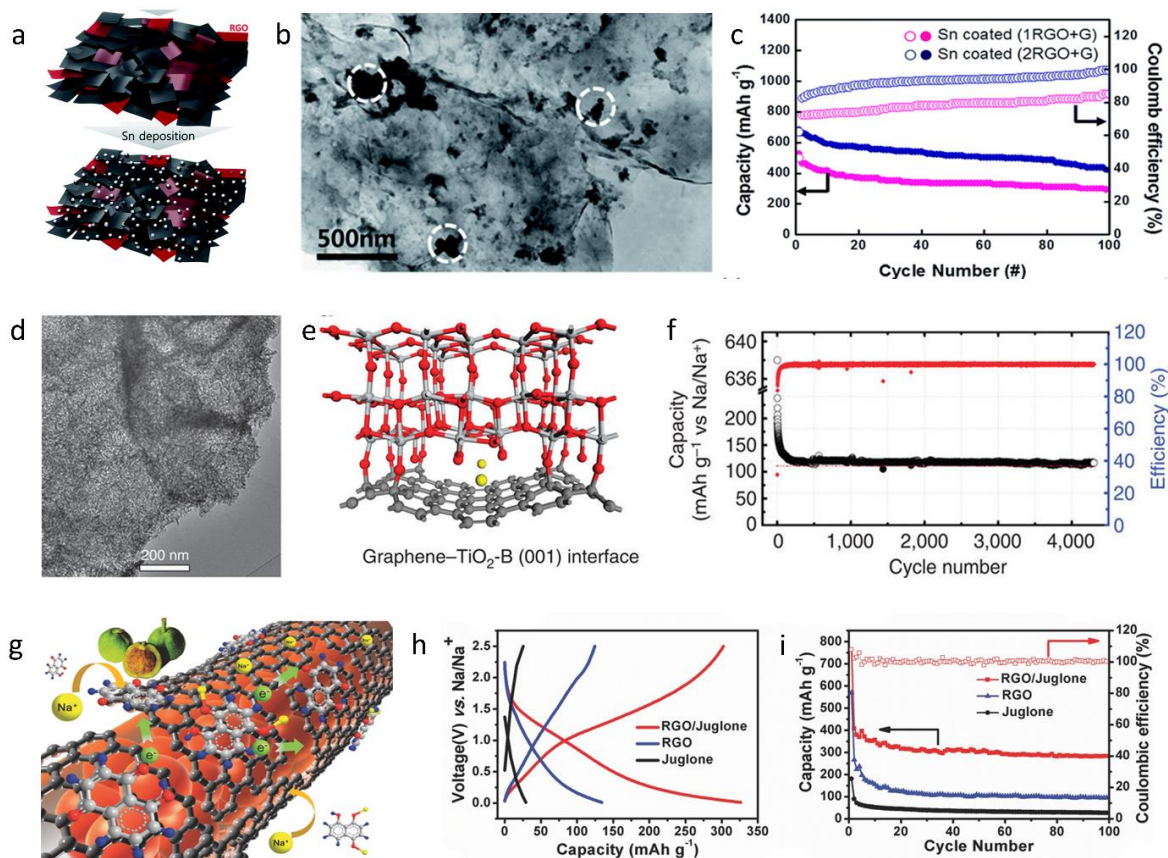
Figure 5. (a) Schematic illustration of Na storage in graphite, graphene oxide and expanded graphite, (b) charge/discharge profiles for the 2nd cycles of pristine graphite (PG), graphene oxide (GO), expanded-graphite 1h (EG-1h) and EG-5h, (c) long term cyclic stability of EG-1h (EG);[88] (d) simulation results of fully sodiated GO with ½ epoxide/hydroxyl mixture structure and epoxide-only structure, corresponding to capacities of 372 and 930 mAh g-1, respectively.[89] (a-c) Reproduced with permission.[88] Copyright 2014, Nature Publishing Group. (d) Reproduced with permission.[89] Copyright 2015, American Chemical Society.
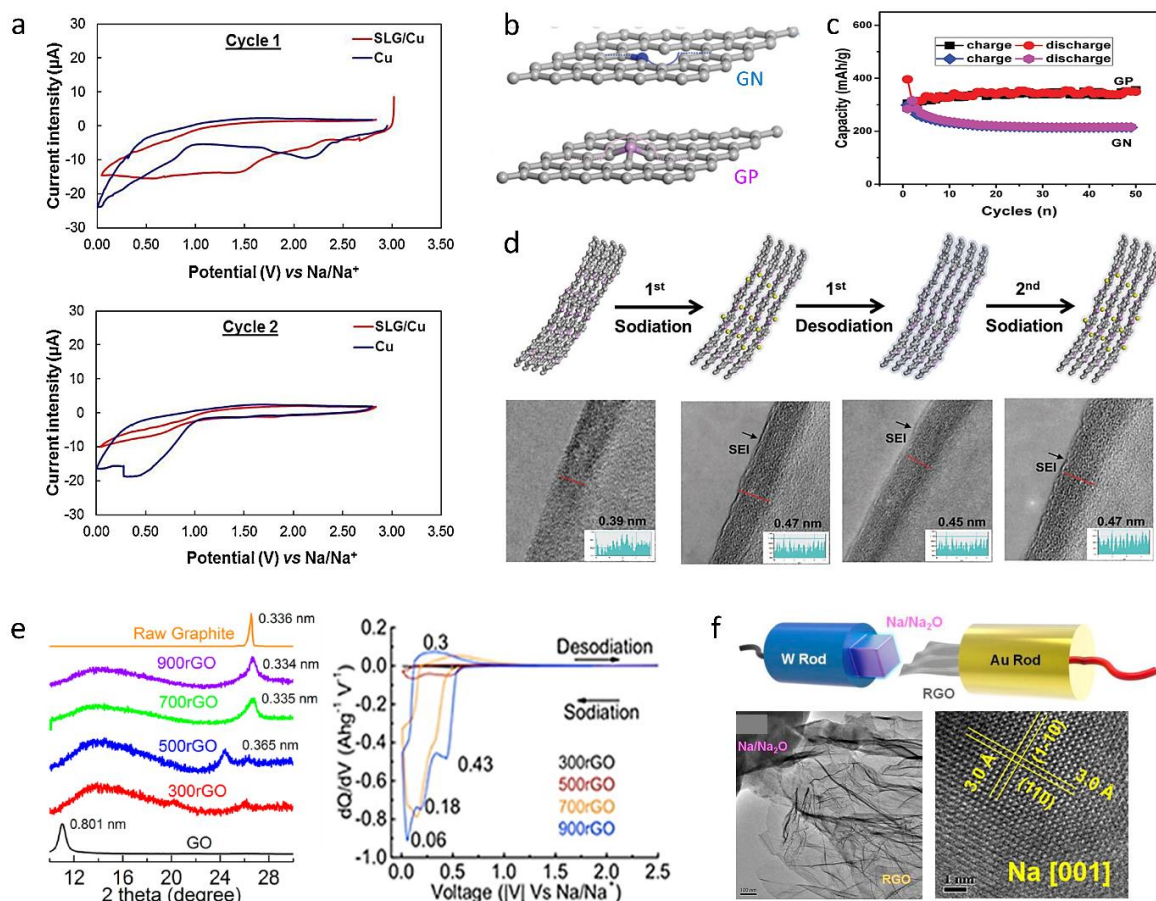
Figure 6. (a) First two cycles cyclic voltammetry (CV) curves of bare Cu and single layered graphene/Cu (SLG/Cu) electrodes in SIBs;[92] (b) schematic illustration of nitrogen-doped graphene (GN) and phosphorus doped graphene (GP), (c) the cyclic capacities of GN and GP electrodes, (d) sodiation/desodiation processes of GP observed by *in-situ* TEM;[95] (e) XRD patterns of rGO annealed at different temperatures and the corresponding CV curves to show Na storage capacity of different rGO specimens;[102] (f) formation of Na metal in rapid-rGO during discharge observed by *in-situ* TEM.[104] (a) Produced with permission.[92] Copyright 2015, Elsevier. (b-d) Produced with permission.[95] Copyright 2017, Royal Society of Chemistry. (e) Reproduced with permission.[102] Copyright 2014, American Chemical Society. (f) Reproduced with permission. [104] Copyright 2016, American Chemical Society.

Figure 7. (a) Schematic illustration of the Sn depiction on GO sheets, (b) TEM image of Sn/rGO composite, (c) the cyclic capacities and Coulombic efficiencies of Sn/rGO composite electrodes;[111] (d) TEM image of graphene/TiO$_2$ composite, (e) schematic diagram of the bonded graphene-TiO$_2$ interface with fast Na ion diffusion path along the [010] direction, (f) the long-term cyclic performance of graphene/TiO$_2$ at 0.5 A g^{-1};[113] (g) schematic diagram for the π-π interaction between rGO sheets and the Juglone molecule, (h) capacity-voltage profiles and (i) cyclic capacities of rGO, Juglone and rGO/Juglone electrodes.[114] (a-c) Reproduced with permission.[111] Copyright 2016, Royal Society of Chemistry. (e-f) Reproduced with permission.[113] Copyright 2015, Nature Publishing Groups. (g-i) Reproduced with permission.[114] Copyright 2015, Wiley-VCH.

Table 1. Electrochemical performance of reported graphitic carbon material anodes in SIBs.

Materials	ICE/ %	Cyclability/ mAh g^{-1}	Rate capability/ mAh g^{-1}	Ref.
Graphite	~54	150 at 0.1 A g^{-1} for the 1st cycle 100 at 0.5 A g^{-1} after 2500 cycles	150 at 0.1 A g^{-1}, 100 at 5 A g^{-1}, 75 at 10 A g^{-1}	[52]
Graphite	~86	~100 at 37.2 mA g^{-1} for the 1st cycle, ~87 at 37.2 mA g^{-1} after 100 cycles	~100 at 37.2 mA g^{-1}, ~80 at 372 mA g^{-1}	[53]
Graphene foam	~54	~150 at 0.2 A g^{-1} for the 1st cycle ~120 at 12 A g^{-1} after 8000 cycles	~150 at 1 A g^{-1}, ~125 at 10 A g^{-1} and ~100 at 30 A g^{-1}	[56]
Graphite	~90	110 at 0.1 A g^{-1} for the 1st cycle ~110 at 0.2 A g^{-1} after 6000 cycles	~110 at 0.1 A g^{-1}, ~102 at 10 A g^{-1}	[70]
Carbon black	~62	234 at 50 mA g^{-1} for the 1st cycle 72 at 3.2 A g^{-1} after 2000 cycles	196 at 0.1 A g^{-1}, 259 at 0.4 A g^{-1} and 105 at 3.2 A g^{-1}	[71]
Expanded graphite	66	120 at 0.12A g^{-1} for the 1st cycle 115 at 0.12A g^{-1} after 100 cycles	120 at 0.12A g^{-1}, 78.2 at 0.24 A g^{-1}	[72]
Expanded graphite	49.3	284 at 0.02A g^{-1} for the 1st cycle 136 at 0.1A g^{-1} after 2000 cycles	284 at 0.02A g^{-1}, 184 at 0.1A g^{-1}, 91 at 0.2A g^{-1}	[88]
P-doped graphene	~75	372 at 0.025 A g^{-1} after 120 cycles	210 at 0.5 A g^{-1}	[95]
N-doped expanded carbon	73.6	482.1 at 0.1 A g^{-1} for the 1st cycle 303.2 at 0.5 A g^{-1} after 700 cycles	327.8 at 0.5 A g^{-1}, 242 at 1 A g^{-1}, 192.5 at 2A g^{-1}, 119.5 at 5 A g^{-1}	[96]
S-doped graphene	23	325 at 0.05 A g^{-1} for the 1st cycle 343 at 0.05 A g^{-1} after 200 cycles	472 at 0.05A g^{-1}, 310 at 0.1 A g^{-1}, 241 at 0.2 A g^{-1}, 182 at 1A g^{-1} and 168 at 2A g^{-1}	[97]
B-doped graphene	63	280 at 0.02 A g^{-1} for the 1st cycle 117 at 1 A g^{-1} after 5000 cycles	212 at 0.08 A g^{-1}, 176 at 0.2 A g^{-1} and 153 at 0.4 A g^{-1}	[98]
N-doped graphene foam	42.6	852 at 0.5 A g^{-1} for the 1st cycle 594 at 0.5 A g^{-1} after 150 cycles	815 at 0.5A g^{-1}, 467 at 1A g^{-1}, 245 at 2A g^{-1}, 138 at 5A g^{-1}	[99]
N, S-doped graphene	50.8	269 at 0.1A g^{-1} for the 1st cycle 260 at 1A g^{-1} after 10000 cycles	400 at 0.03A g^{-1}, 141 at 5 A g^{-1}	[100]
rGO	~24	~180 at 0.2 A g^{-1} for the 1st cycle 141 at 0.04 A g^{-1} after 1000 cycles	176.4 at 0.08 A g^{-1}, 150.9 at 0.2 A g^{-1}, 118.7 at 0.4 A g^{-1}, 95.6 at 1A g^{-1}	[101]
rGO paper	~24	122 at 0.1 A g^{-1} for the 1st cycle ~100 at 0.1A g^{-1} after 1000 cycles	115 at 0.1 A g^{-1} and 52 at 2.4 A g^{-1}	[102]
Holey rGO	22	220 at 0.03 A g^{-1} for the 5th cycle ~140 at 0.1 A g^{-1} after 500 cycles	160 at 0.5A g^{-1}, 144 at 1Ag^{-1}, 104 at 5A g^{-1}, 85 at 10A g^{-1}	[103]

Rapid rGO	18.5	450 at 0.025 A g^{-1} for the 1st cycle 200 at 0.25 A g^{-1} after 750 cycles	316 at 0.05 A g^{-1}, 237 at 0.125 A g^{-1}, 194 at 0.25 A g^{-1} and 162 at 0.5 A g^{-1}	[104]
Crumped rGO	~33	183 at 0.1 A g^{-1} for the 1st cycle ~100 at 1A g^{-1} after 500 cycles	~200 at 0.1 A g^{-1}, 81 at 8 A g^{-1}	[105]
Sn/rGO	62	615 at ~0.3 A g^{-1} for the 1st cycle ~450 at ~0.3A g^{-1} after 100 cycles	~600 at 0.03 A g^{-1}, ~400 at 0.6 A g^{-1}, 200 at 6 A g^{-1} and ~175 at 12 A g^{-1}	[111]
Phosphorene-rGO	~80	1178 at 0.05A g^{-1} for the 1st cycle 1004 at 0.05A g^{-1} after 100 cycles	700 at 8A g^{-1}, 579 at 12 A g^{-1}, 444 at 20 A g^{-1} and 311 at 26 A g^{-1}	[112]
TiO_2-rGO	31.4	~250 at 0.05A g^{-1} for the 1st cycle ~120 at 0.5A g^{-1} after 4300 cycles	287 at 0.2 A g^{-1}, 149 at 0.5 A g^{-1}, 125 at 1.5 A g^{-1}, 114 at 3A g^{-1} and 102 at 6 A g^{-1}	[113]
Juglone-rGO	57.8	440 at 0.1A g^{-1} for the 1st cycle 280 at 0.1A g^{-1} after 100 cycles	398 at 0.05 A g^{-1}, 250 at 0.2 A g^{-1}, 225 at 0.3 A g^{-1} and 210 at 0.4 A g^{-1}	[114]

Biographies
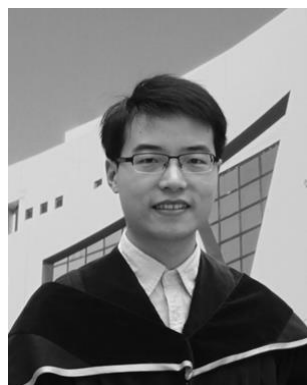
Zheng-Long Xu received his B.Sc degree in Materials Science and Engineering from Zhejiang University in 2012 and PhD degree in Mechanical and Aerospace Engineering from the Hong Kong University of Science and Technology in 2016. He is currently a Korea Research Fellow (KRF) at Seoul National University. His research interests lie in the design of nanomaterials for energy storage systems and *in-situ* transmission electron microscopy studies.

Jooha Park received his B.S. degree in materials science and engineering from Seoul National University in 2017. He is currently working as Ph.D. student in Prof. Kang's group in the Department of Materials Science and Engineering, Seoul National University, South Korea. His research interest focuses on graphite intercalation compounds for energy storage systems.

Kisuk Kang is a professor of materials science and engineering at Seoul National University (SNU), where he received his B.Sc. He completed his Ph.D. and postdoctoral studies at the Massachusetts Institute of Technology. Since 2013, he has been a tenured professor at SNU. His research laboratory focuses on developing new materials for batteries and electrocatalyst using combined experiments and ab initio calculations.

Graphitic carbon materials are promising anodes for the burgeouing sodium ion battery (SIB) technology. An overview of the state-of-art achievements in graphitic carbon anode materials for SIBs is summarized. New findings of sodium storage mechianisms are highlighted, associated with discussion of the correlation between micrsotructures and electrochemical performance. Perspectives for applicable SIBs are also presented.

Sodium Ion Battery

Z. L. Xu, J. Park, G. Yoon, H. Kim and K. Kang*

Graphitic carbon materials for advanced sodium ion batteries

ToC:

41